I.A.U
Karaj branch

Journal of
A p p l ied
C hemical
R esearch
jacr.kiau.ac.ir

Journal of Applied Chemical Research, 16, 4, 63-80 (2023)

Synthesis, characterization and Microwave Absorption Properties of Novel Hard-soft Ferrite and Polyaniline-loaded Nanocomposite

Tolou Pourashraf [1], Mohammad Yousefi[2,*], Saeid Shokri [3], Abbas Ahmadi [4], Parviz Aberoomand Azar[5]

[1]Department of Chemistry, Science and Research Branch, Islamic Azad University, Tehran, Iran

[2]Department of Chemistry, Faculty of Pharmaceutical Chemistry, Tehran Medical Sciences, Islamic Azad University, Tehran, Iran

[3]Digital Transformation Center, Research Institute of Petroleum Industry (RIPI), Tehran, Iran

[4]Department of Chemistry, Faculty of Science, Karaj Branch, Islamic Azad University, Karaj, Iran

[5]Department of Chemistry, Science and Research Branch, Islamic Azad University, Tehran, Iran

(Received 08 Feb. 2023; Final revised received 26 May 2023)

Abstract

Nanocomposites of hard-soft ferrites $(SrFe_{12}O_{19})_{(1-x)}/(Ni_{0.4}Mn_{0.2}Zn_{0.4}Fe_2O_4)_x$ with x = 0.2, 0.4, 0.6, and 0.8 are synthesized by the auto-combustion sol-gel method. In-situ polymerization is used to create polyaniline and hard-soft ferrite nanocomposites. X-ray powder diffractometers (XRD), field emission scanning electron microscopes (FESEM), Fourier transform infrared spectra (FTIR), vibrating sample magnetometers (VSM), and vector network analyzers (VNA) have all been used to evaluate the structure, morphology, magnetic properties, and microwave absorption of nanocomposites. FT-IR spectra are used to confirm and validate the existence of both tetrahedral and octahedral complexes, as well as the interactions between polymer chains and hard and soft nanoparticles, which show that ferrite nanocomposites are coated with polymers. In hard-soft and polymeric nanocomposites, XRD analysis reveals the presence of pure hard and soft phase characteristics as well as PANI characteristics. SEM images show that the particles agglomerate in hard-soft composites as the soft phase rises as a result of being magnetic, and images for polymeric composites show cohesive PANI particles that surround the hard-soft ferrite particle's surface. These findings demonstrate that PANI and hard-soft ferrites can be properly connected. VSM analysis revealed that by adding polymers, the magnetic properties of hard-soft composites dropped

significantly due to the nonmagnetic effects of PANI. The VNA test shows that PANI/$(SrFe_{12}O_{19})_{0.4}$/$(Ni_{0.4}Mn_{0.2}Zn_{0.4}Fe_2O_4)_{0.6}$ exhibits optimized reflection loss from -1.84 to -16.53 in the X-Band (8-12.5 GHz frequency range) when compared to $(SrFe_{12}O_{19})_{0.4}$/$(Ni_{0.4}Mn_{0.2}Zn_{0.4}Fe_2O_4)_{0.6}$ with a matching thickness of 3 mm.

Keywords: Hard-soft nanocomposites, Hexagonal ferrite, Polyaniline, Magnetic properties, Microwave absorption.

---

*__Corresponding author__: *Mohammad Yousefi, Department of Chemistry, Faculty of Pharmaceutical Chemistry, Tehran Medical Sciences, Islamic Azad University, Tehran, Iran. Email: myousefi50@hotmail.com.*

Introduction

Magnetic nanocomposites with hard and soft phases are difficult to design in the scientific world. The two phases of magnetic nanocomposites are usually ferro- or ferromagnetic, with magnetic and structural variations [1, 2]. The key features of hard-soft composites are high coercivity in the hard phase and high saturation and residual magnetization in the soft phase [3, 4]. In recent years, researchers have been working on improving the properties of one of the hard-soft composite designs, combining hexagonal ferrite as the hard phase and spinel ferrite as the soft phase. The hard and soft phases are each suitable for some demands. The spinel phase is used for microwave applications, and the hexagonal ferrite is used for high anisotropy and high resonant frequency applications. Thus, by developing a hard-soft composition, it is possible to create a composite with both properties that can be employed for both high and low anisotropy demands [5-7]. The special properties can be greatly enhanced by changing the synthesis processes, incorporating impurities, or replacing them in composite structures [8].

The microwave absorption and magnetic characteristics of hard-soft composites, with a focus on exchange coupling, have been reported as one of the most challenging issues in hard-soft composites. $NiFe_2O_4/SrCo_{0.2}Fe_{11.8}O_{19}$ [9], $(Ba_{0.5}Sr_{0.5}Fe_{12}O_{19})_{1\_x}(CoFe_2O_4)_x$ [10], $Mn_{0.6}Zn_{0.4}Fe_2O_4/Sr_{0.85}Ba_{0.15}Fe_{12}O_{19}$ [11], $Ni_{0.5}Zn_{0.5}Fe_2O_4/SrFe_{12}O_{19}$ [12], $SrFe_{12}O_{19}/Ni_{0.5}Zn_{0.5}Fe_2O_4$ [13], $SrFe_{12}O_{19}/Ni_{0.7}Zn_{0.3}Fe_2O_4$ [14], $BaFe_{12}O_{19}/Ni_{0.8}Zn_{0.2}Fe_2O_4$ [15], $BaFe_{12}O_{19}/Y_3Fe_5O_{12}$[16], $SrFe_{12}O_{19}/NiFe_2O_4/ZnFe_2O_4$ [17], $SrFe_{10}Al_2O_{19}/Co_{0.8}Ni_{0.2}Fe_2O_4$ [18], and $SrFe_{12-x}V_xO_{19}/(Ni_{0.5}Mn_{0.5}Fe_2O_4)_y$ [19] are examples of hard-soft composites that have been considered. Investigations were conducted on the aforementioned composites' magnetic and microwave properties as well as the effects of phase ratio and various hard and soft phase compositions.

Pahwa et al. synthesized the hard-soft ($BaFe_{12}O_{19}/NiFe_2O_4$) composites using two different processing methods: single-step technique and physical mixing. The nanocomposites were studied at various weight ratios. The results showed that when the $NiFe_2O_4$ concentration increased, microwave absorption characteristics declined at 12–18 GHz. Furthermore, it was demonstrated that single-step composites with higher frequency reflection loss (RL) peaks are better suited to construct exchange-coupled systems [20]. Another study looked at the microwave properties of exchange-coupled $BaFe_{12}O_{19}/Ni_{0.5}Zn_{0.5}Fe_2O_4$ nanocomposites with different weight ratios. The RL frequency was discovered to be dependent on soft phase content, with the largest loss occurring at 13.8 GHz. The obtained results revealed that the exchange-coupling greatly affected RL frequency and levels [21]. The investigation on microwave absorption of $(Ba_{0.5}Sr_{0.5}Fe_{12}O_{19})_{1-x}/(NiFe_2O_4)_x$ (x

= 0.1-0.4) was presented by Mathews et al. in [22]. It was discovered that the minimal RL for sintered composites was higher than that for pure hard and soft phases.

Han et al. investigated the microwave absorption characteristics of $Ni_{0.5}Zn_{0.5}Fe_2O_4/SrFe_{12}O_{19}$ composites with respect to the mass ratio variation. Microwave absorption characteristics in the 2–18 GHz range were shown to be strongly reliant on both soft and hard phase mass ratios, as well as sample thickness. It was also discovered that the fraction of $SrFe_{12}O_{19}$ in the compound increased real permittivity, which is usually caused by strontium hexaferrite's high uniaxial anisotropy and coercivity. They reported that the exchange-coupling effect and microwave properties of the compound were determined by the mass ratio of the hard and soft phases [12].

A variety of hard-soft nanocomposites ($SrFe_{12}O_{19}/MCe_{0.04}Fe_{1.96}O_4$; M = Cu, Zn, Mn, Co, and Ni) were studied in another study on the microwave characteristics of the composite and the composition of the soft phase. Spinel ferrites made of Mn and Ni exhibited the strongest electromagnetic absorption. The ones chosen in the soft phase have various electronic shell shapes and ionic radii, which may be the cause of this issue [23].

According to the literature, magnetic properties and exchange coupling are closely related to microwave absorption properties. It is feasible to improve microwave properties by modifying the exchange coupling, followed by the magnetic properties. Due to complex synthesis techniques and microstructural issues, the exchange coupling concept in hard-soft ferrites has been difficult to realize [24]. New challenges also appear when working with polycrystalline nanocomposites [25]. The difficult-to-quantify and control grain morphologies, size distribution, and relative crystallite orientations all have a significant contribution [16, 26].

These problems and limitations emphasize the necessity for additional study on hard-soft nanocomposites. In the current work, novel hard-soft compositions in different phase ratios were investigated for their microstructural, magnetic, and microwave properties. To that end, hard-soft composites with novel compositions $(SrFe_{12}O_{19})_{(1-x)}/(Ni_{0.4}Mn_{0.2}Zn_{0.4}Fe_2O_4)_x$ were synthesized using the sol-gel auto-combustion procedure. After that, in-situ polymerization was used to form the composite $PANI/(SrFe_{12}O_{19})_{(1-x)}/(Ni_{0.4}Mn_{0.2}Zn_{0.4}Fe_2O_4)_x$ (x = 0.2, 0.4, 0.6, 0.8) with the purpose of enhancing microwave absorption properties. These components are unique and can have remarkable electric and electromagnetic capabilities, resulting in materials with interesting features.

Experimental

Materials

Ammonium peroxydisulfate ($(NH_4)_2S_2O_8$, APS), iron nitrate nonahydrate ($Fe(NO_3)_3.9H_2O$), strontium nitrate ($Sr(NO_3)_2$), zinc nitrate tetrahydrate ($Zn(NO_3)_2.4H_2O$), nickel nitrate hexahydrate

($Ni(NO_3)_2.6H_2O$), manganese nitrate hexahydrate ($Mn(NO_3)_2.4H_2O$), citric acid ($C_6H_8O_7.H_2O$), and aniline monomer were utilized without any further purification.

Preparation of $(SrFe_{12}O_{19})_{(1-x)}/(Ni_{0.4}Mn_{0.2}Zn_{0.4}Fe_2O_4)$

The auto-combustion sol-gel method was used to synthesize $(SrFe_{12}O_{19})_{(1-x)}/(Ni_{0.4}Mn_{0.2}Zn_{0.4}Fe_2O_4)_x$ ferrite composites. Two batches each of spinel ferrite and hexaferrite solutions were prepared using this method. In this way, iron nitrate and strontium nitrate were first dissolved in stoichiometric ratios in deionized water, and the temperature was raised to 80 °C until a clear solution was obtained. Citric acid was added to the solution in a 1:1.5 ratio so that it did not precipitate, and the mixture was then cooled at room temperature. The spinel ferrite solution was then poured over the hexaferrite solution and heated. Citric acid was added again in the same ratio and vigorously mixed, and ammonia was added to the solution to adjust the pH. At this point, the solution's color had changed to green. The temperature was increased to 180 °C after the pH was adjusted. Furthermore, as the temperature rises, auto-combustion occurs, and the solution turns into a black powder. The powder obtained during the two stages of the calcination process (one hour at 500 °C and two hours at 1200 °C) will be annealed in the furnace.

Preparation of PANI/$(SrFe_{12}O_{19})_{(1-x)}/(Ni_{0.4}Mn_{0.2}Zn_{0.4}Fe_2O_4)$

In-situ polymerization was used to synthesize polymer composites $(PANI/(SrFe_{12}O_{19})_{(1-x)}/(Ni_{0.4}Mn_{0.2}Zn_{0.4}Fe_2O_4)_x)$. For this, 5 g of ammonium peroxydisulfate was dissolved in 30 cc of hydrochloric acid in a beaker. In another beaker, 0.3 g of pre-prepared hard-soft ferrite, 1 cc aniline, and 64 cc hydrochloric acid were stirred for 30 minutes. At a low speed, an ammonium peroxydisulfate solution was added to the aniline-ferrite solution. The solution was placed in an ice bath for 24 hours and stirred at a constant speed to complete the polymerization process. After the polymerization process was completed, the polymer was filtered and washed with acid and deionized water.

Characterization

Fourier-transform infrared spectroscopy (FTIR, Tensor 27 Bruker) with a KBr tablet was used to identify compounds. The structure of nanocomposites was examined using X-ray diffraction (XRD) (Model: XPERT-MPD, Philips) in the 2θ range of a 10- to 80-degree angle with a step size of 0.5 and Cu Kα radiation (λ = 1.5418). To observe the morphology of the materials, a field emission scanning electron microscope (FESEM, SIGMA, VP-500, ZEISS model) was used. A Lake Shore 7307 vibrating sample magnetometer (VSM) was employed to analyze the magnetic characteristics and hysteresis loops. In the X-band frequency range (8–12 GHz), microwave absorption was evaluated using a vector network analyzer (VNA, Agilent 8510C). Composites and paraffin were

combined in a 70/30 mass ratio to suit compounds for tests of electromagnetism absorption. The samples were formed using a rectangular mold that had dimensions of 22.86 by 10.16 by 1 mm3.

Table 1 clearly shows the specimen codes of the samples.

Characterization

Fourier-transform infrared spectroscopy (FTIR, Tensor 27 Bruker) with a KBr tablet was used to identify compounds. The structure of nanocomposites was examined using X-ray diffraction (XRD) (Model: XPERT-MPD, Philips) in the 2θ range of a 10- to 80-degree angle with a step size of 0.5 and Cu Kα radiation (λ = 1.5418). To observe the morphology of the materials, a field emission scanning electron microscope (FESEM, SIGMA, VP-500, ZEISS model) was used. A Lake Shore 7307 vibrating sample magnetometer (VSM) was employed to analyze the magnetic characteristics and hysteresis loops. In the X-band frequency range (8–12 GHz), microwave absorption was evaluated using a vector network analyzer (VNA, Agilent 8510C). Composites and paraffin were combined in a 70/30 mass ratio to suit compounds for tests of electromagnetism absorption. The samples were formed using a rectangular mold that had dimensions of 22.86 by 10.16 by 1 mm^3.

Table 1. Specimen's codes of samples.

Number	Sample	Sample code
1	$(SrFe_{12}O_{19})_{(0.8)}/(Ni_{0.4}Mn_{0.2}Zn_{0.4}Fe_2O_4)_{(0.2)}$	20% Soft
2	$(SrFe_{12}O_{19})_{(0.6)}/(Ni_{0.4}Mn_{0.2}Zn_{0.4}Fe_2O_4)_{(0.4)}$	40% Soft
3	$(SrFe_{12}O_{19})_{(0.4)}/(Ni_{0.4}Mn_{0.2}Zn_{0.4}Fe_2O_4)_{(0.6)}$	60% Soft
4	$(SrFe_{12}O_{19})_{(0.2)}/(Ni_{0.4}Mn_{0.2}Zn_{0.4}Fe_2O_4)_{(0.8)}$	80% Soft
5	$PANI/(SrFe_{12}O_{19})_{(0.8)}/(Ni_{0.4}Mn_{0.2}Zn_{0.4}Fe_2O_4)_{(0.2)}$	20% + PANI
6	$PANI/(SrFe_{12}O_{19})_{(0.6)}/(Ni_{0.4}Mn_{0.2}Zn_{0.4}Fe_2O_4)_{(0.4)}$	40% + PANI
7	$PANI/(SrFe_{12}O_{19})_{(0.4)}/(Ni_{0.4}Mn_{0.2}Zn_{0.4}Fe_2O_4)_{(0.6)}$	60% + PANI
8	$PANI/(SrFe_{12}O_{19})_{(0.2)}/(Ni_{0.4}Mn_{0.2}Zn_{0.4}Fe_2O_4)_{(0.8)}$	80% + PANI

Results and Discussion

XRD Analysis

Figure 1 depicts the X-ray diffraction (XRD) of the synthesized samples. In this way, the XRD patterns of $(SrFe_{12}O_{19})/(Ni_{0.4}Mn_{0.2}Zn_{0.4}Fe_2O_4)_x$ (Figure 1a), PANI/ $(SrFe_{12}O_{19})/(Ni_{0.4}Mn_{0.2}Zn_{0.4}Fe_2O_4)_x$ (Figure 1b), pure soft (Figure 1c), and pure hard (Figure 1d) were displayed. The observed peaks were analyzed using their matching Miller indices. The intensity and positions in the obtained XRD peaks of pure hard were validated with a standard file (reference code: 96-152-7076, a = b = 5.7800, c = 22.9800, and V_{cell} = 667.85, space group P63/mmc). The resulted XRD peaks for pure soft were also validated with a standard file (Reference code: 96-154-1590, a = b = c = 8.3420, and V_{cell} = 580.51, space group Fd-3m), which confirms cubic structure. From the XRD data of the synthesized samples, in the soft ferrite (cubic ferrite), a = 8.236, while in the hard ferrite (hexagonal ferrite), a = 5.448 and c = 23.023. Both samples' (pure hard and soft ferrites) lattice parameters are properly close to the numbers reported. The comparison of Figure 1a to Figure 1c and Figure 1d clearly shows that the characteristic peaks for soft and hard ferrites are visible in all composites $(SrFe_{12}O_{19})/(Ni_{0.4}Mn_{0.2}Zn_{0.4}Fe_2O_4)_x$ with different contents of soft and hard ferrites. The peak at 2θ = 35.57 corresponds to the 311 plane for soft ferrite ($Ni_{0.4}Mn_{0.2}Zn_{0.4}Fe_2O_4$). As shown in Figure 1d, hard ferrite ($SrFe_{12}O_{19}$) has a characteristic peak at 2θ = 34.38 for the 114 plane. Small changes in the relative intensity and position of the diffraction peaks for ferrites were observed as a result of the substitution.

In all composites, the hard and soft phase XRD patterns match, indicating that the peaks of both phases are well formed and placed together [27, 28]. The XRD pattern of hard-soft nanocomposites with polyaniline conductive polymer (PANI/ $(SrFe_{12}O_{19})/(Ni_{0.4}Mn_{0.2}Zn_{0.4}Fe_2O_4)$) in Figure 1b demonstrates that all peaks of the prepared samples match up to the hard and soft phase characteristics. The peak corresponding in 2θ = 25.4 is related to polyaniline formation. In general, the amorphous peak of polyaniline is apparent in the XRD pattern of polymeric nanocomposite, in addition to the XRD pattern of ferrites. Furthermore, the intensity of the peaks of polymer nanocomposites is higher than that of pure ferrite nanocomposites. That is due to the polymer coating influencing the ferrite structure, verifying the formation of this nanocomposite [29].

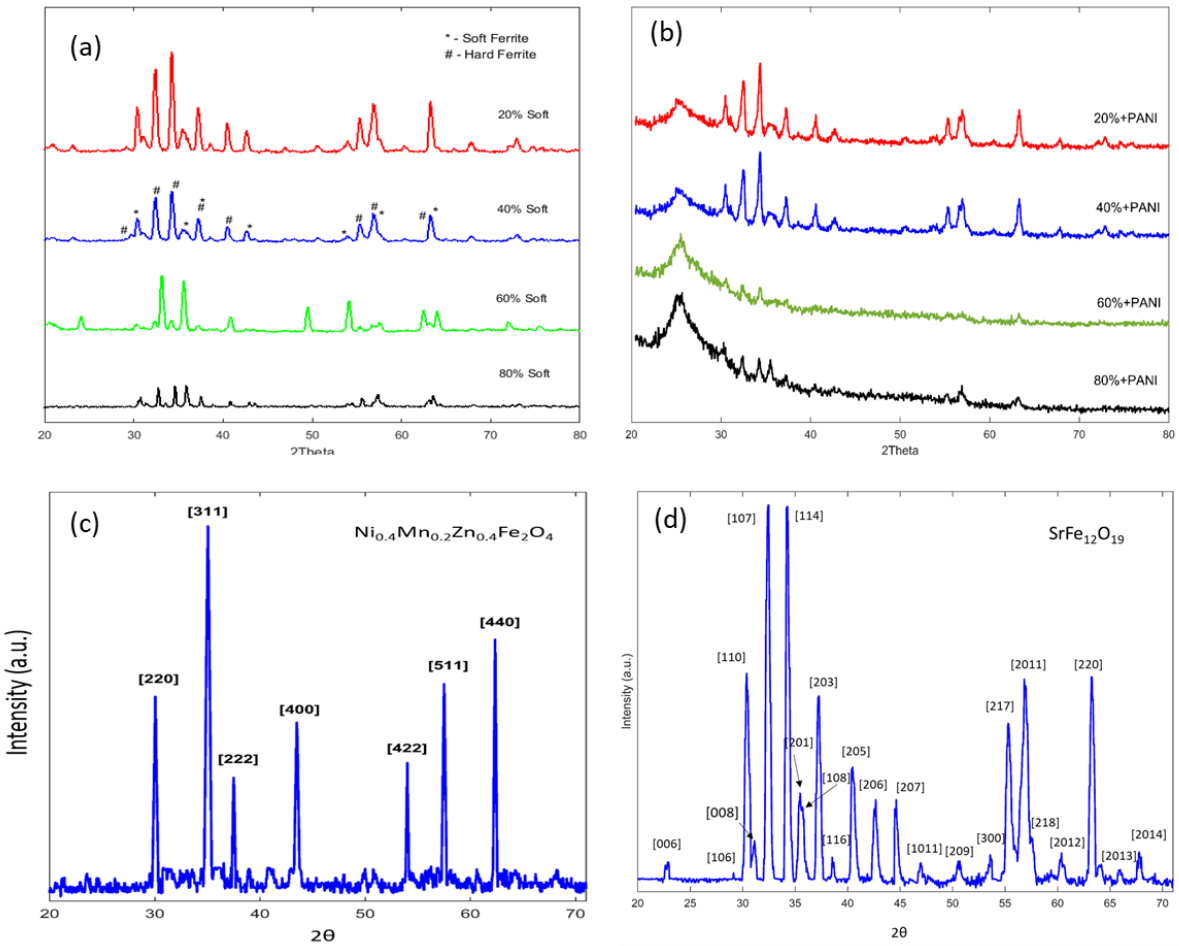

Figure 1. (a): XRD patterns of $(SrFe_{12}O_{19})_{(1-x)}/(Ni_{0.4}Mn_{0.2}Zn_{0.4}Fe_2O_4)_x$, (b): XRD patterns of PANI/$(SrFe_{12}O_{19})_{(1-x)}/(Ni_{0.4}Mn_{0.2}Zn_{0.4}Fe_2O_4)_x$, (c): XRD patterns of pure soft $(Ni_{0.4}Mn_{0.2}Zn_{0.4}Fe_2O_4)$, (d): XRD patterns of pure hard $(SrFe_{12}O_{19})$.

IR Spectra

The FTIR spectra of nanocomposites are depicted in Figure 2. Figure 2a displays nanocomposites of $(SrFe_{12}O_{19})_{(1-x)}/(Ni_{0.4}Mn_{0.2}Zn_{0.4}Fe_2O_4)_x$ with varying soft phase weight percentages.

The stretching vibration of iron and strontium bonds with oxygen is represented in FTIR in the range of about 536–610 cm^{-1} and 440-500 cm^{-1}. These bands are due to metal-oxygen stretching bonds (Fe-O) in the tetrahedral and octahedral, respectively. The bands at 1049 cm^{-1} and 1115 cm^{-1} observed in 60% and 80% of soft phases are related to the C-N bond formation that occurs during the synthesis process of strontium ferrite composites. In the FTIR spectra of all percentages of soft phases, the typical bands of 400–800 cm^{-1} were observed that are related to metal-oxygen absorption bonds, which confirms the hexagonal structure of $SrFe_{12}O_{19}$ for all samples [30].

Figure 2b represents the FTIR spectrum of the PANI/$(SrFe_{12}O_{19})_{(1-x)}$/ $(Ni_{0.4}Mn_{0.2}Zn_{0.4}Fe_2O_4)_x$ nanocomposite. The absorption bands at about 430 and 580 cm^{-1} correspond to stretching vibrations of the Fe-O bond in octahedral and tetrahedral cavities, respectively. Polyaniline has the following

characteristic bands: 1620 cm^{-1} (stretching vibration of the C=C bond in the quinonide ring), 1562 cm^{-1} (stretching vibration of the C=C bond in the benzenoid ring), 1296 cm^{-1} (vibration of the C-H bond in the benzoid ring), 1125 cm^{-1} (stretching vibration N = N of the quinoid ring), and 800 cm^{-1} (bending vibration of the C-H bond in the polyaniline chain) [31, 32]. When polymer is coated on ferrite nanocomposites, the polymer's characteristic bands in the composite are similar to those of pure polyaniline, but their location is slightly shifted, as shown in Figure 2b. The interaction of hard and soft nanoparticles with polymer chains is indicated by these displacements [33].

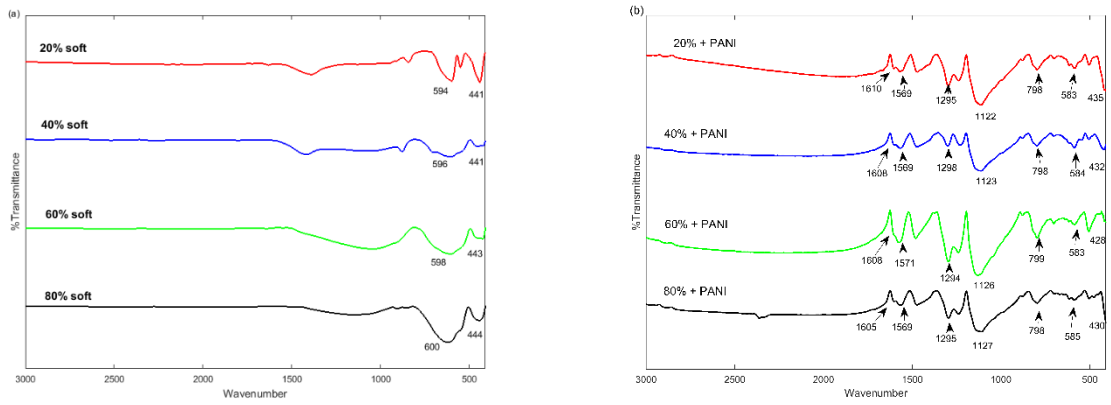

Figure 2. (a): FTIR spectra of $(SrFe_{12}O_{19})_{(1-x)}/(Ni_{0.4}Mn_{0.2}Zn_{0.4}Fe_2O_4)_x$, (b): FTIR spectra of $PANI/(SrFe_{12}O_{19})_{(1-x)}/(Ni_{0.4}Mn_{0.2}Zn_{0.4}Fe_2O_4)$.

Morphology

SEM was employed for morphological studies. Figure 3 depicts SEM images of $(SrFe_{12}O_{19})_{(1-x)}/(Ni_{0.4}Mn_{0.2}Zn_{0.4}Fe_2O_4)_x$ composites calcined at 1200°C, while Figure 4 depicts $PANI/(SrFe_{12}O_{19})_{(1-x)}/(Ni_{0.4}Mn_{0.2}Zn_{0.4}Fe_2O_4)_x$ composites. The presence of two sizes of particles in the images indicates the coexistence of both phases. The hard ferrite grains are distributed uniformly throughout the volume and appear to be absorbed on the surface of the composite's soft ferrite particles. The hard ferrite particles are evenly distributed and surrounded by soft ferrite particles, resulting in a good composite system with good grain bonding [34]. Furthermore, the particles agglomerate as the soft phase of the material increases due to magnetism.

Figure 4 shows FESEM micrographs of the $PANI/(SrFe_{12}O_{19})_{(1-x)}/(Ni_{0.4}Mn_{0.2}Zn_{0.4}Fe_2O_4)$ composite phases that are proportionately dispersed. The granular particles are cubic spinel particles, whereas the plate-like particles are hexagonal. A consistent layer of polyaniline is formed on the top of hard-soft particles after coating them with PANI [35]. Figure 4 shows unified PANI particles that are completely covered by the composite's surface. Due to the harsher surface of

polymer-hard-soft composites compared to just hard-soft, PANI coated the surface of $(SrFe_{12}O_{19})_{(1-x)}/(Ni_{0.4}Mn_{0.2}Zn_{0.4}Fe_2O_4)_x$ [36].

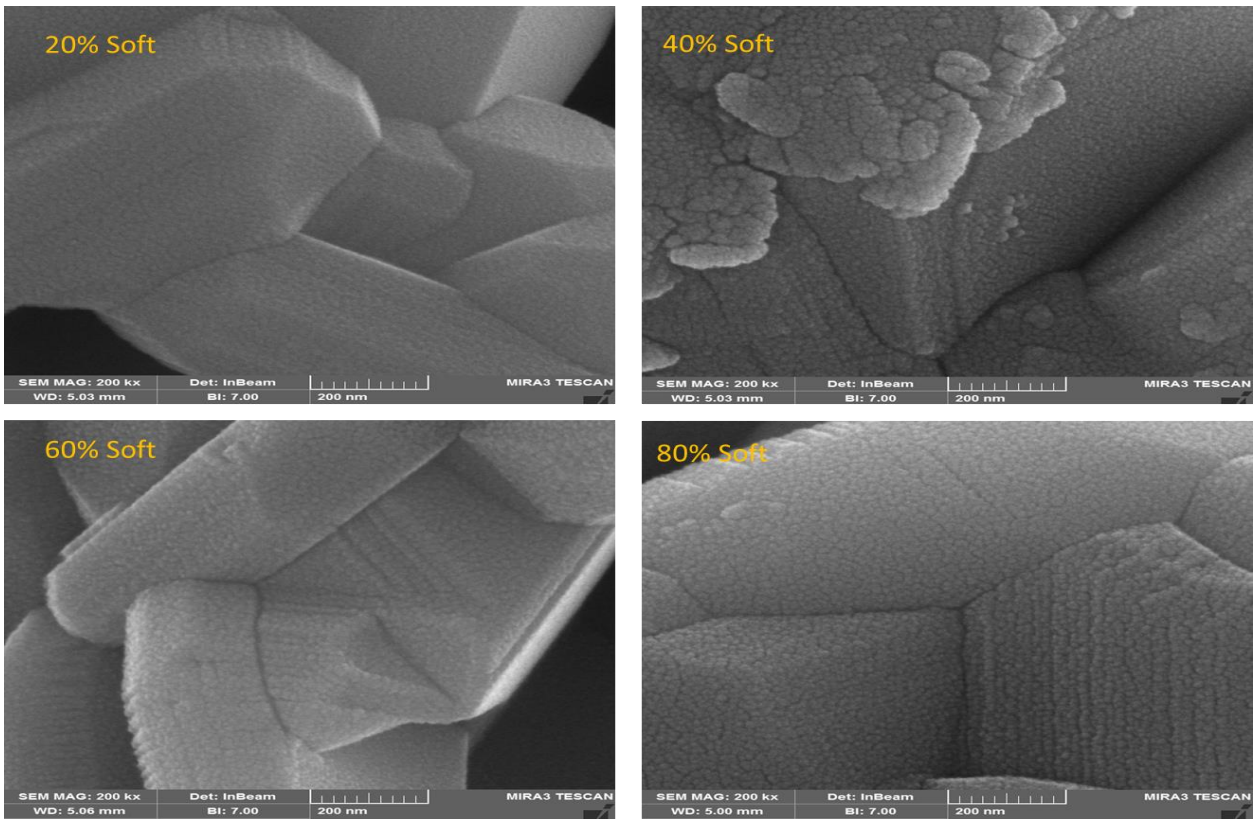

Figure 3. FESEM micrograph of hard-soft ferrite $((SrFe_{12}O_{19})_{(1-x)}/(Ni_{0.4}Mn_{0.2}Zn_{0.4}Fe_2O_4)_x)$ nanocomposites with different weight ratios of soft ferrite.

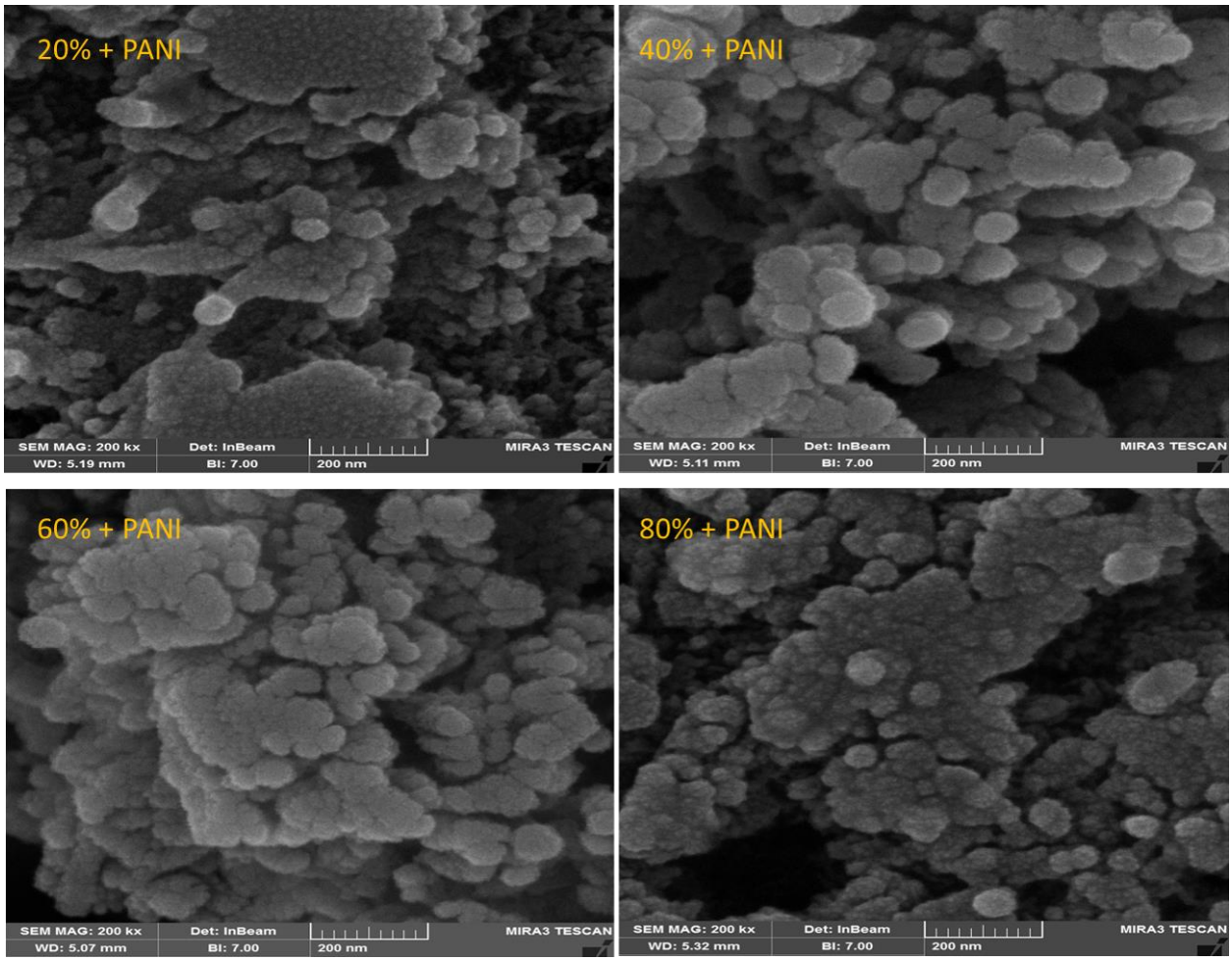

Figure 4. FESEM micrograph of hard-soft ferrite/PANI (PANI/$(SrFe_{12}O_{19})_{(1-x)}$/ $(Ni_{0.4}Mn_{0.2}Zn_{0.4}Fe_2O_4)_x$) nanocomposites with different weight ratios of soft ferrite.

Magnetic Properties

The hysteresis loops of soft-hard ($(SrFe_{12}O_{19})_{(1-x)}$/$(Ni_{0.4}Mn_{0.2}Zn_{0.4}Fe_2O_4)_x$) vs. polymeric nanocomposites (PANI/$(SrFe_{12}O_{19})_{(1-x)}$/$(Ni_{0.4}Mn_{0.2}Zn_{0.4}Fe_2O_4)_x$) are depicted in Figure 5. The blue dashed line represents soft-hard ferrites, and the solid red line represents polymeric composites.

The hysteresis loop in hard-soft nanocomposites is smooth and unbroken, denoting that the phases have good exchange coupling. Magnetism is dependent on the hard and soft phases. In the presence of a magnetic field, magnetic materials with hard and soft phases can exchange four types of energy: exchange energy, magnetostatic energy, anisotropy energy, and magnetic exchange. Soft magnetic phases are dominated by magnetostatic energy, while hard magnetic phases are dominated by anisotropy energy. The exchange of forces in soft and hard phases can be weak or powerful based on both phases' inherent properties, including grain size, particle shape, and distribution [30, 37]. According to the VSM results of hard-soft composites, high amounts of soft phase weaken the exchange force on the soft grains and increase the dipole interaction. In low nuclear fields, inverse domains in the soft phases can easily nucleate. This will result in less residue in all composites.

When nonmagnetic PANI was placed in the hard-soft phase, the saturation magnetization decreased with increasing soft phase. Lessening the magnetic portion of ferrite resulted in a decrease in saturation magnetization, according to the Ms = φ. ms equation [38], in which Ms is referred to as the volume fraction of the particles (φ) and the saturation moment of a single particle [29]. The nonmagnetic PANI was revealed to split the magnetic grains, resulting in a boost in diamagnetic power effects and a decrease in magnetic properties. The presence of PANI in composites causes a greater separation of magnetic grains. All of this results in a bigger and more powerful demagnetic effect and a weaker magnetic effect in the composites. The composites' coercive force has not changed dramatically. Coercivity is influenced by a variety of factors, including crystalline structure, grain shape, content, and scalability. PANI is accumulated on the ferrite surface and crystallite boundary during polymerization, which decreases the magnetic surface anisotropy of particles. Charge transfer, on the other hand, can occur on the particles' surfaces between ferrite and PANI, where it varies the charge density and impacts the system's electronic spin mechanism. All of these things reduce the domain wall movements that have resulted in a decrease in the coercive force of composites [39]. First, during the polymerization, PANI is accumulated on the surface and crystallite boundaries of the hard-soft composites, resulting in an interaction influence between the PANI and $(SrFe_{12}O_{19})_{(1-x)}/(Ni_{0.4}Mn_{0.2}Zn_{0.4}Fe_2O_4)_x$, and thus the surface anisotropy of the polymeric composites decreases [38]. Second, decreasing the anisotropy field in hexagonal strontium ferrites causes a lower resonance frequency [40, 41]. The PANI covering on hard-soft composites will most likely influence the anisotropy of surface, shape, and interface to net anisotropy [42]. As a result, polymeric composites have less coercivity than hard-soft ones.

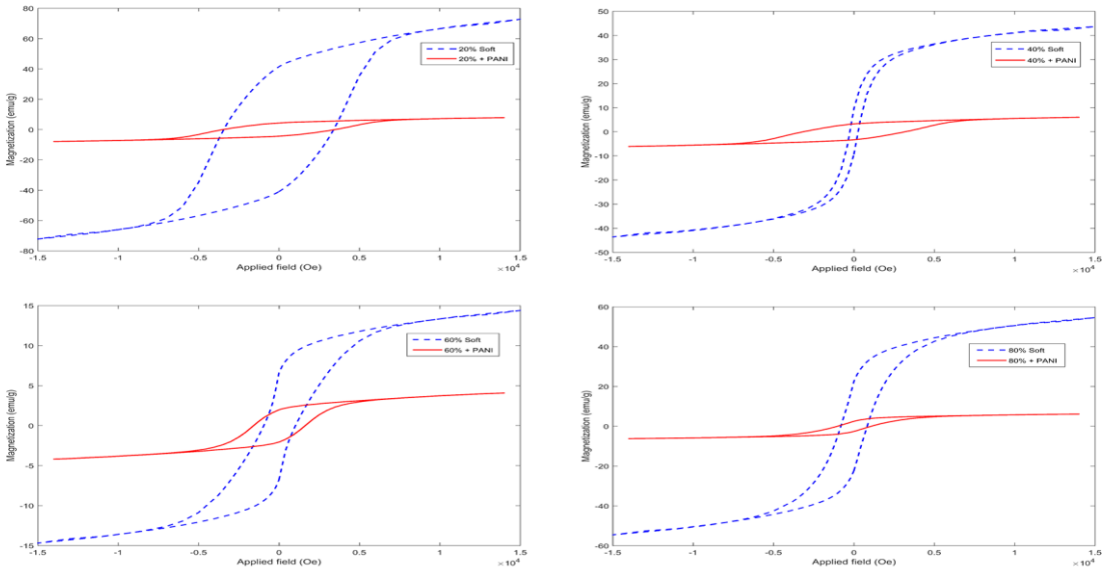

Figure 5. Magnetic hysteresis loops of $(SrFe_{12}O_{19})_{(1-x)}/(Ni_{0.4}Mn_{0.2}Zn_{0.4}Fe_2O_4)_x$ vs. PANI/ $(SrFe_{12}O_{19})_{(1-x)}/(Ni_{0.4}Mn_{0.2}Zn_{0.4}Fe_2O_4)$ with varying soft ferrite weight ratios.

Microwave Absorption

The reflection loss was used to describe the microwave absorptivity of synthesized composites. Eq. 1 is frequently used to determine the normalized input impedance of a microwave absorptive layer using transmission line theory. Where Z_0 denotes the intrinsic impedance, ε and μ denote the complex relative permittivity and permeability, *f* the wave frequency, *d* the thickness, and *c* the velocity of light in vacuum [43, 44]. Eq. 2 presents the RL as a function of the normalized input impedance [45].

$$Z_{in} = Z_0\sqrt{\frac{\mu_r}{\varepsilon_r}}tanh\left[j\frac{2\pi fd}{c}\sqrt{\mu_r\varepsilon_r}\right] \quad (1)$$

$$\mathrm{RL(dB)} = 20\log_{10}\left|\frac{Z_{in}-Z_0}{Z_{in}+Z_0}\right| \quad (2)$$

Figure 6 depicts the frequency dependence of reflection loss and absorption percentage in hard-soft and polymeric composites for each weight percentage. Figure 6a reveals that the reflection loss for the synthesized hard-soft nanoparticles is not desirable at all frequencies ranging from 8 to 12 GHz. However, at 9.145 GHz, the composite with 60% soft phase has the highest percentage of absorption and the lowest RL_{min}, with values of 34.63 and -1.8460, respectively. Based on the results, it is clear that the composite $SrFe_{12}O_{19}/Ni_{0.4}Mn_{0.2}Zn_{0.4}Fe_2O_4$ with an 80% soft phase does not absorb correctly in the X band. Waves can be absorbed more effectively by reducing the soft phase in the X band. Figure 6b also shows that the polymeric composite samples have more than 50% absorption throughout the X band. The sample that has 60% soft phase at 9.75 GHz, yielded the best results, with an absorption percentage of 76.4% and a reflection loss of -16.53. The slope of the diagram at the end of the X band of RL and the absorption percentage at the frequency of 12.4 GHz are notable in these diagrams, especially in composites with 20% soft phase, where they are -17.9% and 92.5%, respectively. Another important point in the 60% soft phase PANI/$SrFe_{12}O_{19}/Ni_{0.4}Mn_{0.2}Zn_{0.4}Fe_2O_4$ composites is that the absorption percentage is between 64 and 77 across the X bandwidth, whereas in the 20% soft phase PANI/$SrFe_{12}O_{19}/Ni_{0.4}Mn_{0.2}Zn_{0.4}Fe_2O_4$ composite, the absorption percentage is between 58 and 92.5. According to the findings of microwave absorption in polymeric composites, the electrical conductivity of polyaniline was found to improve absorption properties when compared to hard-soft composites. The conclusion is that this composite, with its moderate absorption and broad bandwidth, can be used as an absorbent material for microwaves in the X-band range.

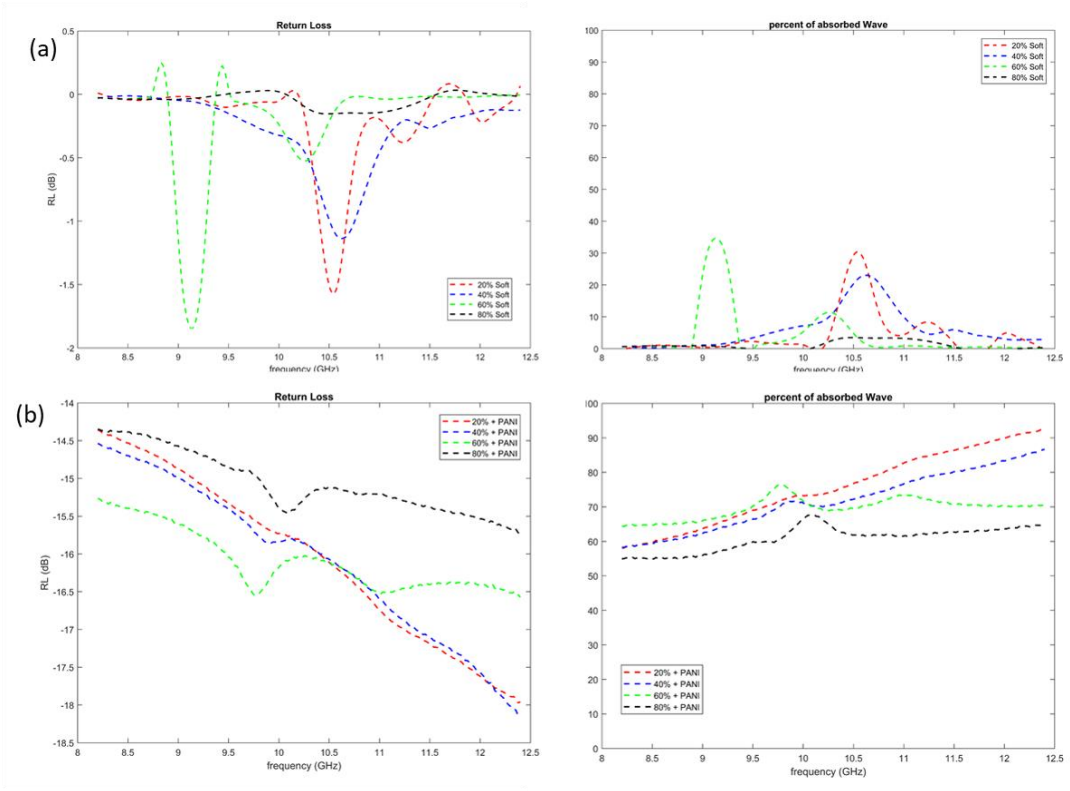

Figure 6. Frequency dependence of reflection loss and absorption percentage of (a): $(SrFe_{12}O_{19})_{(1-x)}/(Ni_{0.4}Mn_{0.2}Zn_{0.4}Fe_2O_4)_x$ and (b): $PANI/(SrFe_{12}O_{19})_{(1-x)}/(Ni_{0.4}Mn_{0.2}Zn_{0.4}Fe_2O_4)_x$.

Conclusions

Hard-soft ferrite $(SrFe_{12}O_{19})_{(1-x)}/(Ni_{0.4}Mn_{0.2}Zn_{0.4}Fe_2O_4)_x$) was successfully developed by auto-combustion sol-gel. After that, three-component composites with PANI ($PANI/(SrFe_{12}O_{19})_{(1-x)}/(Ni_{0.4}Mn_{0.2}Zn_{0.4}Fe_2O_4)_x$) were prepared by in-situ polymerization. The simplicity of obtaining the initial materials and the lack of demanding steps required in the preparation process are the two most important benefits of the auto-combustion sol-gel approach. This approach has shown its ability to produce nanocomposites with a variety of compositions and can operate in an open environment. Overall, nanocomposites of polymeric hard-soft ferrites and hard-soft ferrite were created using a straightforward and affordable method. The composites' morphological and structural characteristics demonstrate how they were formed. In addition, unlike the hard-soft composites that did not have excellent absorption in the X band frequencies, all polymeric composites in this study had better absorption percentages (lower RL). Therefore, it is reasonable to conclude that the produced composites are suitable for EMI shielding.

One technique to improve the qualities of ferrites is to substitute cations in particular places in their structure. However, there are issues with replacing certain cationic sites, which are usual in many doped oxides. This matter should be thoroughly investigated in future research. In the study of novel compounds, more precise information regarding the mechanical and thermal resistance of

ferrites will be helpful. In addition, because ferrites are widely used in high-frequency applications, future research should concentrate on establishing a new way of power loss analysis.

References

1. Mathews SA, Babu DR, Saravanan P, Hayakawa Y. Microwave absorption studies of (Ba0. 5Sr0. 5Fe12O19) 1-x/(NiFe2O4) x hard/soft ferrite nanocomposites. Materials Chemistry and Physics. 2020;252:123063.

2. Sudhakaran A, Sudhakaran A, Sivasenthil E. Investigating structure, elasticity, morphology, composition, and optical behavior of Al-doped BaFe12O19/CoZnFe2O4 hybrid composite. Journal of Materials Research. 2023;38(5):1239-53.

3. Qie Y, Liu Y, Kong F, Yang Z, Yang H. Exchange-Coupling of Hard/Soft Magnetic Phases of Co/FeCo Nanocomposites. The Journal of Physical Chemistry C. 2022;126(20):8826-31.

4. Yousefi M, Afghahi S, Amini M, Torbati MB. An investigation of structural and magnetic properties of Ce–Nd doped strontium hexaferrite nanoparticles as a microwave absorbent. Materials Chemistry and Physics. 2019;235:121722.

5. Sudhakaran A, Sudhakaran A, Sivasenthil E. Multifunctionality of AlBaFe12O19/CoZnFe2O4 hybrid nanocomposite: Promising structural, elastic, morphological, compositional, optical, and magnetic properties. Journal of Physics and Chemistry of Solids. 2023;174:111134.

6. Mortazavinik S, Yousefi M. Preparation, magnetic properties and microwave absorption of Zr–Zn–Co substituted strontium hexaferrite and its nanocomposite with polyaniline. Russian Journal of Applied Chemistry. 2017;90:298-303.

7. Mesdaghi S, Yousefi M, Mahdavian A. The effect of PANI and MWCNT on magnetic and photocatalytic properties of substituted barium hexaferrite nanocomposites. Materials Chemistry and Physics. 2019;236:121786.

8. Beheshti KA, Yousefi M. Magnetic and microwave absorption of BaMgxZrxFe12-2xO19 polyaniline nanocomposites. Journal of Alloys and Compounds. 2021;859:157861.

9. Xia J, Ning Y, Luo Y, Chen W, Wu X, Wu W, et al. Structural and magnetic properties of soft/hard NiFe 2 O 4@ SrCo 0.2 Fe 11.8 O 19 core/shell composite prepared by the ball-milling-assisted ceramic process. Journal of Materials Science: Materials in Electronics. 2018;29:13903-13.

10. Harikrishnan V, Vizhi RE. A study on the extent of exchange coupling between (Ba0. 5Sr0. 5Fe12O19) 1− x (CoFe2O4) x magnetic nanocomposites synthesized by solgel combustion method. Journal of Magnetism and Magnetic Materials. 2016;418:217-23.

11. Xia J, Shen Y, Xiao C, Chen W, Wu X, Wu W, et al. Structural and Magnetic Properties of Soft/Hard Mn 0.6 Zn 0.4 Fe 2 O 4@ Sr 0.85 Ba 0.15 Fe 12 O 19 Core/Shell Composite Synthesized by the Ball-Milling-Assisted Ceramic Process. Journal of Electronic Materials. 2018;47:6811-20.

12. Han Q, Meng X, Lu C. Exchange-coupled Ni0. 5Zn0. 5Fe2O4/SrFe12O19 composites with enhanced microwave absorption performance. Journal of Alloys and Compounds. 2018;768:742-9.

13. Song F, Shen X, Liu M, Xiang J. Magnetic hard/soft nanocomposite ferrite aligned hollow microfibers and remanence enhancement. Journal of colloid and interface science. 2011;354(1):413-6.

14. Radmanesh M, Ebrahimi SS. Synthesis and magnetic properties of hard/soft SrFe12O19/Ni0. 7Zn0. 3Fe2O4 nanocomposite magnets. Journal of magnetism and magnetic materials. 2012;324(19):3094-8.

15. Roy D, Shivakumara C, Kumar PA. Observation of the exchange spring behavior in hard–soft-ferrite nanocomposite. Journal of magnetism and magnetic materials. 2009;321(5):L11-L4.

16. López-Ortega A, Estrader M, Salazar-Alvarez G, Roca AG, Nogués J. Applications of exchange coupled bi-magnetic hard/soft and soft/hard magnetic core/shell nanoparticles. Physics Reports. 2015;553:1-32.

17. Tyagi S, Baskey HB, Agarwala RC, Agarwala V, Shami TC. Development of hard/soft ferrite nanocomposite for enhanced microwave absorption. Ceramics International. 2011;37(7):2631-41.

18. Torkian S, Ghasemi A, Razavi RS. Magnetic properties of hard-soft SrFe10Al2O19/Co0. 8Ni0. 2Fe2O4 ferrite synthesized by one-pot sol–gel auto-combustion. Journal of Magnetism and Magnetic Materials. 2016;416:408-16.

19. Almessiere MA, Slimani Y, Baykal A. Structural, morphological and magnetic properties of hard/soft SrFe12-xVxO19/(Ni0. 5Mn0. 5Fe2O4) y nanocomposites: effect of vanadium substitution. Journal of Alloys and Compounds. 2018;767:966-75.

20. Pahwa C, Mahadevan S, Narang SB, Sharma P. Structural, magnetic and microwave properties of exchange coupled and non-exchange coupled BaFe12O19/NiFe2O4 nanocomposites. Journal of Alloys and Compounds. 2017;725:1175-81.

21. Jiang C, Liu R, Shen X, Zhu L, Song F. Ni0. 5Zn0. 5Fe2O4 nanoparticles and their magnetic properties and adsorption of bovine serum albumin. Powder technology. 2011;211(1):90-4.

22. Fang G, Liu C, Yang Y, Peng K, Cao Y, Xu G, Zhang Y. High-efficiency microwave absorbing performance originating from sufficient magnetic exchange coupling interaction and impressive dielectric loss. Journal of Materials Chemistry C. 2021;9(6):1936-44.

23. Algarou NA, Slimani Y, Almessiere MA, Alahmari F, Vakhitov M, Klygach D, et al. Magnetic and microwave properties of SrFe12O19/MCe0. 04Fe1. 96O4 (M= Cu, Ni, Mn, Co and Zn) hard/soft nanocomposites. Journal of Materials Research and Technology. 2020;9(3):5858-70.

24. Hernando A, González J. Soft and hard nanostructured magnetic materials. Hyperfine Interactions. 2000;130(1-4):221-40.

25. Arcas J, Hernando A, Barandiarán J, Prados C, Vázquez M, Marín P, Neuweiler A. Soft to hard magnetic anisotropy in nanostructured magnets. Physical Review B. 1998;58(9):5193.

26. Almessiere MA, Slimani Y, Trukhanov A, Sadaqat A, Korkmaz AD, Algarou NA, et al. Review on functional bi-component nanocomposites based on hard/soft ferrites: structural, magnetic, electrical and microwave absorption properties. Nano-Structures & Nano-Objects. 2021;26:100728.

27. Hazra S, Ghosh BK, Patra MK, Jani RK, Vadera SR, Ghosh NN. A novel 'one-pot'synthetic method for preparation of (Ni0. 65Zn0. 35Fe2O4) x–(BaFe12O19) 1− x nanocomposites and study of their microwave absorption and magnetic properties. Powder technology. 2015;279:10-7.

28. Feng H, Bai D, Tan L, Chen N, Wang Y. Preparation and microwave-absorbing property of EP/BaFe12O19/PANI composites. Journal of Magnetism and Magnetic Materials. 2017;433:1-7.

29. Jiang J, Ai L, Li L. Synthesis and characterization of polyaniline-based nanocomposites containing magnetic Li–Ni–La ferrite. Journal of non-crystalline solids. 2009;355(34-36):1733-6.

30. Tavakolinia F, Yousefi M, Afghahi SSS, Baghshahi S, Samadi S. Synthesis of novel hard/soft ferrite composites particles with improved magnetic properties and exchange coupling. Processing and Application of Ceramics. 2018;12(3):248-56.

31. Li Z-F, Zhang H, Liu Q, Liu Y, Stanciu L, Xie J. Covalently-grafted polyaniline on graphene oxide sheets for high performance electrochemical supercapacitors. Carbon. 2014;71:257-67.

32. Hosseini SH, Mohseni S, Asadnia A, Kerdari H. Synthesis and microwave absorbing properties of polyaniline/MnFe2O4 nanocomposite. Journal of Alloys and Compounds. 2011;509(14):4682-7.

33. Tavakolinia F, Yousefi M, Afghahi SSS, Baghshahi S, Samadi S. Effect of Polyaniline on Magnetic and Microwave Absorption Properties in SrFe 12 O 19/Zn 0.4 Co 0.2 Ni 0.4 Fe 2 O 4 Ferrite Nanocomposites. Journal of Inorganic and Organometallic Polymers and Materials. 2020;30:4014-26.

34. Almessiere M, Slimani Y, Attia H, Sheikh S, Sadaqat A, Vakhitov M, et al. Alterations in the magnetic and electrodynamic properties of hard-soft Sr0. 5Ba0. 5Eu0. 01Fe12O19/NixCuyZnwFe2O4 nanocomposites. journal of materials research and technology. 2021;15:1416-29.

35. Sozeri H, Kurtan U, Topkaya R, Baykal A, Toprak MS. Polyaniline (PANI)–Co0. 5Mn0. 5Fe2O4 nanocomposite: Synthesis, characterization and magnetic properties evaluation. Ceramics International. 2013;39(5):5137-43.

36. Liangchao L, Haizhen Q, Yuping W, JIANG J, Feng X. Preparation and magnetic properties of Cu0. 4Zn0. 6Cr0. 5Sm0. 06Fe1. 44O4/polyaniline nanocomposites. Journal of Rare Earths. 2008;26(4):558-62.

37. Dahal JN, Neupane D, Poudel T. Synthesis and magnetic properties of 4: 1 hard-soft SrFe12O19-La1-xSrxMnO3 nanocomposite prepared by auto-combustion method. AIP Advances. 2019;9(7):075308.

38. Chen K, Xiang C, Li L, Qian H, Xiao Q, Xu F. A novel ternary composite: fabrication, performance and application of expanded graphite/polyaniline/CoFe 2 O 4 ferrite. Journal of Materials Chemistry. 2012;22(13):6449-55.

39. Jiang J, Li L, Xu F. Polyaniline–LiNi ferrite core–shell composite: Preparation, characterization and properties. Materials Science and Engineering: A. 2007;456(1-2):300-4.

40. Zhu H, Lin H, Guo H, Yu L. Microwave absorbing property of Fe-filled carbon nanotubes synthesized by a practical route. Materials Science and Engineering: B. 2007;138(1):101-4.

41. Singh P, Babbar V, Razdan A, Puri R, Goel T. Complex permittivity, permeability, and X-band microwave absorption of CaCoTi ferrite composites. Journal of applied physics. 2000;87(9):4362-6.

42. Xu P, Han X, Jiang J, Wang X, Li X, Wen A. Synthesis and characterization of novel coralloid polyaniline/BaFe12O19 nanocomposites. The Journal of Physical Chemistry C. 2007;111(34):12603-8.

43. Kessler Z. Electrical Conductivily in Heterogeneous Polymer. Polymer.12(14):16.

44. Kim S, Jo S, Gueon K, Choi K, Kim J, Churn K. Complex permeability and permittivity and microwave absorption of ferrite-rubber composite at X-band frequencies. IEEE Transactions on Magnetics. 1991;27(6):5462-4.

45. Naito Y, Suetake K. Application of ferrite to electromagnetic wave absorber and its characteristics. IEEE Transactions on Microwave Theory and Techniques. 1971;19(1):65-72.